International Symposium
On Turbulence and Shear Flow
Phenomena (TSFP-9)
June 30 - July 3, 2015 *Melbourne, Australia*

ACTIVE SEPARATION CONTROL PROCESS OVER A SHARP EDGE RAMP

Antoine Debien
Univ. Orléans, INSA-CVL,
PRISME EA 4229,
8 rue Léonard de Vinci
F45072, Orléans, France
antoine.debien@univ-orleans.fr

Sandrine Aubrun
Univ. Orléans, INSA-CVL,
PRISME EA 4229,
F45072, Orléans, France
sandrine.aubrun@univ-orleans.fr

Nicolas Mazellier
Univ. Orléans, INSA-CVL,
PRISME EA 4229,
F45072, Orléans, France
nicolas.mazellier@univ-orleans.fr

Azeddine Kourta
Univ. Orléans, INSA-CVL,
PRISME EA 4229,
F45072, Orléans, France
azeddine.kourta@univ-orleans.fr

ABSTRACT

Pulsed jets vortex generators are used to control a flow separation along a 25° ramp with sharp edge. The actuator optimization is done following the results of previous studies. Before to perform closed loop control, the present study deals with open loop control. In this case, the interactions of the actuation with the separated flow is observed during steady and transient states. The effect of actuation frequency is investigated, including the impact of actuation frequency close to the vortex shedding frequency. The analysis of the separation and the influence of the flow control are based on wall pressure distribution and velocity fields obtained by 2D-2C PIV. Characterization of attachment and separation phases are also investigated. This study shows that the actuator used can reduce significantly the separation zone.

INTRODUCTION

Flow separation occurs in a number of practical situations such as land and flight vehicles and leads often to unwanted nuisances among those performance loss, structural vibrations or noise generation. Active flow control is an attractive solution to mitigate flow separation and has therefore received an increasing interest over the past two decades (Collis *et al.* (2004); Greenblatt & Wygnanski (2000)). Nevertheless, physical mechanisms governing the separated flow and issuing vortices are still not completely characterized to allow to use a suitable control. In addition, the interactions between the actuation and the separated zone are still largely misunderstood. This is a cornerstone issue to design efficient actuators and control laws as well (Gad-el Hak (2007)).

This work aims at describing the turbulent organization of the controlled flow over a backward-facing ramp using counter-rotating pulsed jets, i.e. Active Vortex Generators (AVG). Their design is based on the optimal configuration found by Godard & Stanislas (2006) and Cuvier *et al.* (2011). In the present study, we investigate the effect of the actuation frequency in both steady and transient states.

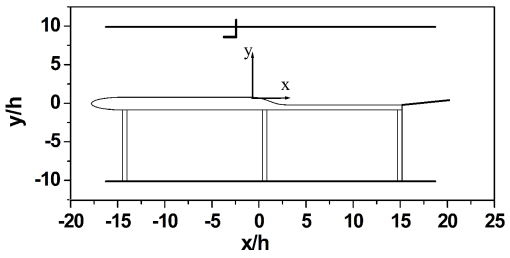

Figure 1. Schematic of the experiment facility.

EXPERIMENTAL SETUP

In the following, we describe briefly the experimental facilities used in this work. More details can be found in Debien *et al.* (2014). Experiments are conducted in the closed loop subsonic wind tunnel of PRISME laboratory characterized by a test section of $5 \times 2 \times 2\ m^3$ (length × width × height). The maximum free stream velocity reachable is 60 $m.s^{-1}$. The free stream turbulence intensity is below 0.4%. In the present case, the freestream velocity is equal to $U_\infty = 20\ m.s^{-1}$. A ramp model is installed at mid-height of the test section and spans the tunnel width (figure 1). The ramp is characterized by a slant angle of 25° ending with a 7^{th} order polynomial (figure 2). Its length l is 470 mm whereas its height h is 100 mm. The origin of the streamwise coordinate x coincides to the sharp edge of the ramp. Close to the sharp edge, a Reynolds number $Re_\theta \approx 3500$ is achieved, based on the momentum thickness ($Re_h \approx 1.3 \times 10^5$, based on the ramp height).

To achieve separation control, 54 counter-rotating Active Vortex Generators (AVGs) are set one boundary layer

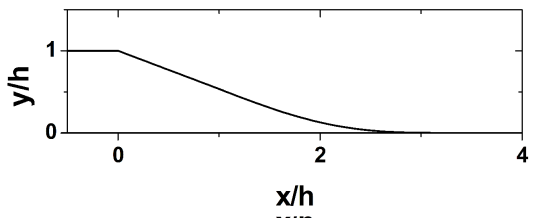

Figure 2. Sketch of sharp edge ramp configuration.

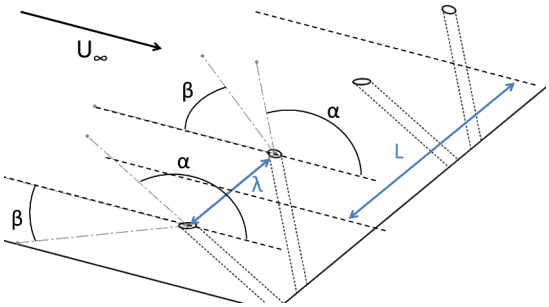

Figure 3. sketch of VGA design.

thickness (δ used in the next paragraph) upstream of the sharp edge. Their design and spatial arrangement are extrapolated from the results reported by Godard & Stanislas (2006) and Cuvier *et al.* (2011) with a jet velocity ratio $V_r = V_{jet}/U_\infty = 3$. Each actuator (figure 3) consists on two counter-rotating jets with a hole $\phi = 1.2$ mm in diameter. They present a pitch angle of $\alpha = 135°$ and a skew angle of $\beta = 45°$. The distance between the two jets of each actuator is $\lambda/\phi = 15$. Between the center lines of two consecutive AVGs, the distance is $L/\phi = 30$. The actuation frequency f_{pulse} has been varied within the range $0.265 \leq f^+ \leq 6.62$ ($f^+ = \frac{f_{pulse} \times L_{sep}}{U_\infty}$, where L_{sep} the length of the separation). In the following, we report two specific cases, i.e. f^+ = 0.795 and f^+ = 1.98 Hz, that lead to similar reduction of the separation region over the ramp. The frequency f^+ = 0.795 is close to the baseline flow vortex shedding frequency (see Debien *et al.* (2014)).

The effects of flow control are investigated through both wall pressure and velocity field measurements. The static pressure distribution along the centerline of the model is obtained using 58 wall pressure taps (0.3 mm in diameter) connected to Electronic pressure scanner (ESP-16HD and ESP-32HD, 2500 $Pa, \pm 0.75$ Pa) acquisition unit. In order to ensure good statistical convergence, the sampling time is set to $T_{aq}U_\infty/\delta = 275,000$ ($T_{aq} = 300$ s) with a 200 Hz sampling frequency.

The measurements of the pressure fluctuations are obtained with four Kulite pressure transducers ($XCQ-62$, 0.29 mV/mBar) operated at a sampling frequency of 20 kHz with a sampling time $T_{aq}U_\infty/\delta = 41,300$ ($T_{aq} = 45$ s). A first pressure sensor is located right downstream from the sharp edge at $x/h = 0.05$, two other sensors are located close to the baseline attachment line, i.e. $x/h = 5.27$ and 5.77, respectively. A last sensor is located in the wake, at $x/h = 6.77$.

2D-2C PIV is used to obtain statistical properties of the velocity field in a streamwise vertical plane located at an upward flow occurring between two counter-rotating vortices

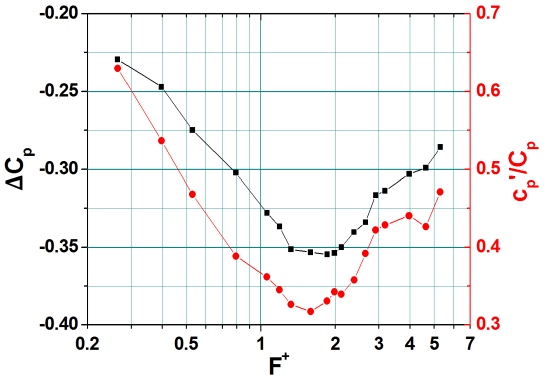

Figure 4. Evolution of mean and rms pressure coefficient downstream of the sharp edge ($x/h = 0.05$) versus f^+ (V_r = 3, DC = 50 %).

produced by AVGs. 2500 pairs of images are recorded to ensure statistical convergence. The statistical errors of the mean and second-order moments are respectively 1% and 3% for a 97% confidence interval. In order to characterize both average and transient states, i.e. attachment (respectively separation) stage occurring when the control is switched on (respectively off), PIV is used to obtain phase-averaged velocity fields. Each phase is averaged over 1000 samples. The statistical errors of the mean and second-order moments are 2% and 5%, respectively, for a 97% confidence interval.

RESULTS AND DISCUSSION

Average State

To focus on the analysis of the impact of AVG actuation frequency, the velocity ratio and the Duty Cycle are set at V_r = 3 and DC = 50 %, respectively. This yields a constant momentum coefficient $C_\mu = 16.5 \times 10^{-4}$ ($C_\mu = \frac{\rho_{jet} DCV_{jet}^2 S_{jet}}{\frac{1}{2}\rho_\infty U_{infty}^2 S_{ref}}$), with ρ_{jet} and ρ_∞ the actuator and free stream flow density, S_{jet} the total area of the actuators and S_{ref} the ramp slant part area).

The variation of the pressure coefficient (C_p) versus f^+ (figure 4) shows that compared to the baseline case, AVGs induce at all frequency range a C_p decrease, due to an acceleration of the near wall flow downstream of the sharp edge. Furthermore, the rms value of C_p (C_p') presents a similar trend versus f^+. Within $0.265 \leq f^+ \leq 1.32$, C_p and C_p' decrease. A plateau with a maximal C_p reduction is observed from $1.32 \leq f^+ \leq 2$. For $2 \leq f^+ \leq 5.3$, C_p and C_p' progressively increases as f^+ increases.

As C_μ is kept constant for the overall frequency range and as pressure sensor is close to the separation point, the variations of C_p properties can be expected to be induced by the separation and shear layer characteristics. Compared to the baseline case, a large decrease of the pressure coefficient for a fixed f^+ should correspond to a deflection of the shear layer towards the wall, expected to promote a reduction of the separation length. Coupled with tuft visualizations, those results have been used to select two cases where the impact of AVG control on flow field is further investigated. The pulsation frequency is set either to f^+ = 1.98 (corresponding to a maximal C_p reduction) or f^+ = 0.795 (leading on tuft visualization), which is close to the natural vortex shedding frequency.

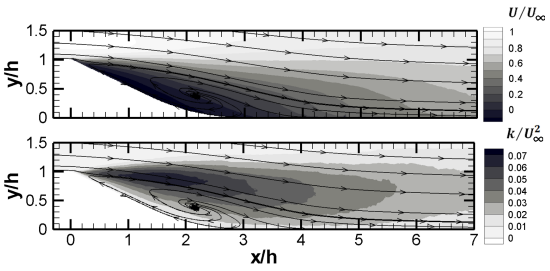

Figure 5. Mean streamwise velocity and turbulent kinetic energy k over the ramp (f^+ = 1.98, $V_r = 3$, DC = 50 %).

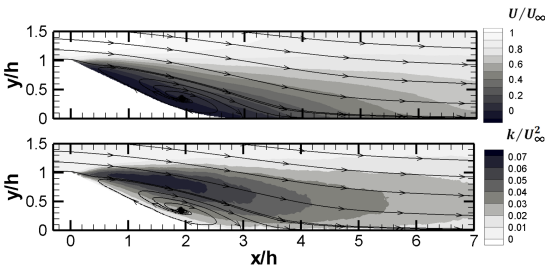

Figure 6. Mean streamwise velocity and turbulent kinetic energy k over the ramp (f^+ = 0.795, $V_r = 3$, DC = 50 %).

The mean velocity field obtained for f^+ = 1.98 (figure 5) presents a near wall streamwise velocity increase upstream of the sharp edge ($\sim$ 3 %), as a consequence of increasing momentum transfer between free and near wall flows imposed by the streamwise vortices (AVGs). Compared to the baseline case, the shear layer developing downstream of the separation point is deflected towards the wall and the mean attachment point is located at $x/h = 3.14$. The drastic reduction of the recirculation zone induces an acceleration of reverse flow close to separation point. this reverse flow acceleration is expected to promote the suction of the shear layer above the wall. Beyond the separation point, the maximum levels of turbulent kinetic energy (TKE) ($\frac{k}{U_\infty^2}$, figure 5) are present in the shear layer. TKE at the separation point presents a value of $\frac{k}{U_\infty^2} = 0.034$. This value progressively increases up to a maximal value located upstream of the recirculation center ($\frac{k}{U_\infty^2}$ = 0.067 at $\{1.4 \leq x/h \leq 1.5; y/h = 0.9\}$). Farther downstream, the TKE progressively decreases. This TKE topology is very different of the baseline case where maximal values are obtained beyond recirculation center. This suggests that interactions between the recirculation bubble and the shear layer are increased with the control. The mean velocity and TKE flow fields when f^+ = 0.795 (figure 6) are very similar to the previous control case and presents a mean attachment point located at x/h = 2.93.

Furthermore, the shear layer evolution is now analyzed using similarity coordinates (figure 7). The reduced coordinate $\eta = \frac{y-y_c}{\delta_\omega}$ is used where y_c corresponds to the position of the maximal velocity gradient and δ_ω to the vorticity thickness of the shear layer. The velocity difference $\Delta U = U_{max} - U_{min}$ is used as reference velocity. For the baseline case (figure 7 (a)), the dimensionless profiles do not show a similarity feature. In particular, the evolution of the back-flow along the ramp seems responsible for the evolution of the lower part of dimensionaless profiles ($\eta \leq 0$).

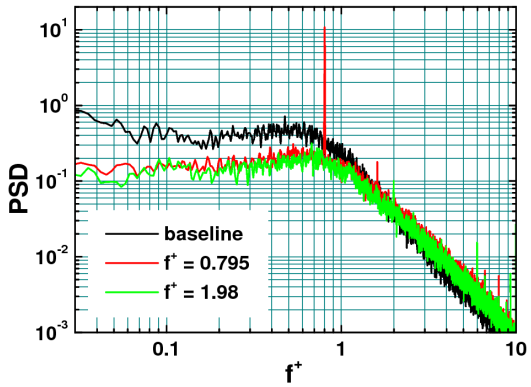

Figure 8. Power Spectra Density (PSD) of the pressure fluctuations ($x/h = 5.77$).

For the controlled cases (figure 7 (b) and (c)), similarity state is achieved close to the separation point. This similarity state is achieved when during the control phase the shear layer development is driven by the growth and the convection of structures induced by AVG blowing.

Both controlled cases lead to a similar drastic reduction of the recirculation region. For f^+ = 1.98, the separation length is decreased by 41% while for f^+ = 0.795 a reduction of the separation length of 48 % is observed. Regarding the C_p reduction observed versus f^+ (figure 4), it appears that, contrary to the separation reduction results, the C_p reduction is greater for f^+ = 1.98 than for f^+ = 0.795 (suggesting a further decrease of separation length for f^+ = 1.98). This means that physical mechanisms underlying separation-actuation interactions differ from one case to another as emphasized by the spectra of unsteady pressure plotted in figure 8. Compared to baseline, controlled cases present lower PSD level at low frequency which is due to the displacement of the attachment point further upstream than pressure sensor location. In the baseline case, these high levels at low frequency are due to low frequency motions, characteristic feature of reattachment zones. For f^+ = 0.795, a large peak is visible at the actuation frequency unlike the case f^+ = 1.98. This large peak can be the signature of two phenomena: transient separation induced by the low frequency actuation or lock-on control, inducing the triggering and shedding of large structures. Furthermore, the convective character of pressure time-series cross-correlation (figure 9) suggests a lock-on for f^+ = 0.795.

This hypothesis is well illustrated by the evolution of phase-averaged velocity fields shown in figure 10 which have been computed when the blowing is turned on (figure 10 (a)) and when it is turned off (figure 10 (b)). When the AVGs start blowing, two structures can be clearly identified. The first one is located at x/h = 0.65 and the second one at x/h = 2.37. When the AVGs blowing are turned off (figure 10 (b)), a large structure is located at x/h = 0.65. These results suggest that the structure location is triggered by actuation, which leads to slightly better control performances since the separation length is further decreased. This lock-on effect induced by the control is present despite the original objective of AVGs to produce streamwise vortices. Furthermore, the visualization of the phase-averaged vorticity fields (see $t^+ = 1.88$ figure 12 or $t^+ = 17$ figure 13) shows that during blowing phase, AVGs lead to deflect the

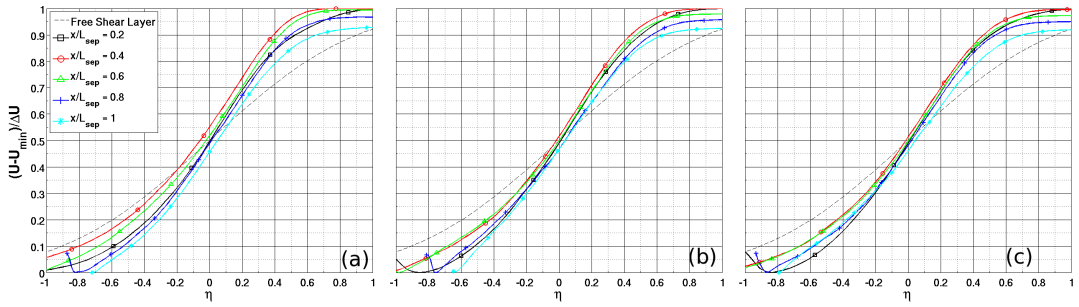

Figure 7. Mean streamwise velocity profiles of the shear layer in similarity coordinates for (a) baseline case, (b) controlled case $f^+ = 0.795$, (c) controlled case $f^+ = 1.98$.

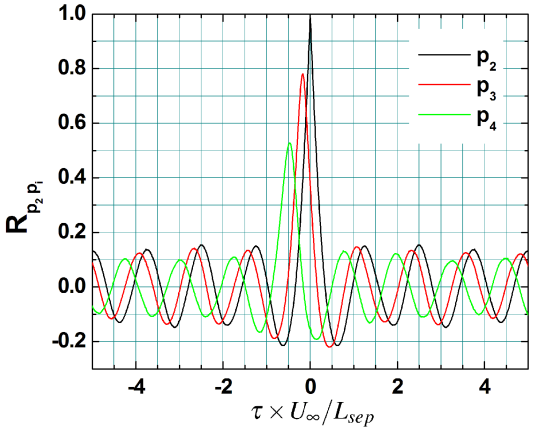

Figure 9. Cross-correlations of the pressure fluctuations ($f^+ = 0.795$, $x/h_{p2} = 5.27$, $x/h_{p3} = 5.77$ and $x/h_{p4} = 6.77$).

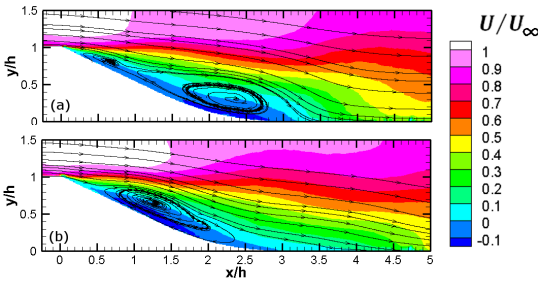

Figure 10. Phase averaged velocity field, $U_0 = 20m/s$, $f^+ = 0.795$. (a) $\varphi = 0$, beginning of blowing phase (b) $\varphi = \pi$, end of blowing phase.

vorticity layer along the ramp up to $x/h \approx 0.73$ despite the sharpness of the edge and the slat angle of the ramp. It is supposed that counter-rotating streamwise vortices dominate the shear layer development up to this position. Beyond $x/h = 0.73$, the classic development of the shear layer with spanwise roll-up process dominates.

Transient states

Attachment and separation transient states induced when actuation is turned on or off is now analyzed. For that purpose, actuation is turned on at $t^+ = 0$ ($t^+ = t \times U_\infty/L_{sep}$)

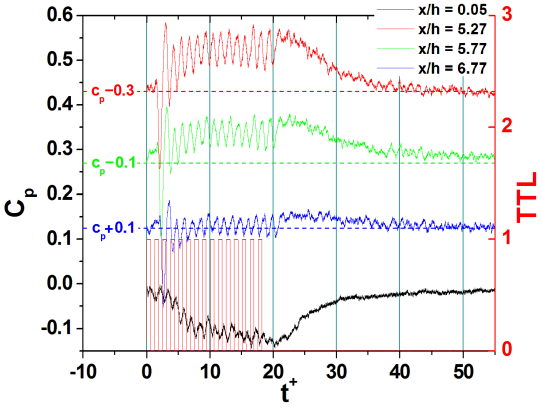

Figure 11. Phase-averaged wall pressure fluctuations for attachment and separation process, $U_0 = 20m/s$, $f^+ = 0.795$.

and then turned off at $t^+ = 18$. The transient processes of attachment and separation mechanisms are highlighted by phase-averaged fluctuation pressure (figure 11). Using the definition of Darabi & Wygnanski (2004*a*), the attachment duration has a time scale of $t^+ \approx 10$ while the separation process has a time scale of $t^+ \approx 20$, which is consistent with Siauw *et al.* (2010). Furthermore, the actuation phase presents large pressure fluctuations with the actuation frequency. Close to the sharp edge, the negative pressure fluctuations are directly related to the blowing AVGs, which induce near the wall a flow acceleration. As mentioned above, control at $f^+ = 0.795$ induces the formation of large coherent structures leading to an increase of pressure fluctuations. This pressure signature is observed close to the mean non-controlled attachment point ($x/h = 5.27$). Pressure fluctuations progressively decrease (see $x/h = 6.77$), which is expected to be due to the destruction of the shear layer large spanwise coherent structures after their impingement to the wall. Furthermore the evolution of the pressure coefficient downstream of the sharp edge presents a monotonic decrease up to the steady actuated state while close to the initial attachment point, a large fluctuation with a similar time scale as the actuation is first observed before a monotonic pressure increase. This large fluctuation is observed at $x/h = 5.27$ (local minimum at $t^+ = 2.1$ and local maximum at $t^+ = 3$) and propagates downstream with a convection velocity $V_c \approx 0.51 \times U_\infty$.

The evolution of the vorticity field during the attachment process is presented in figure 12. As observed above,

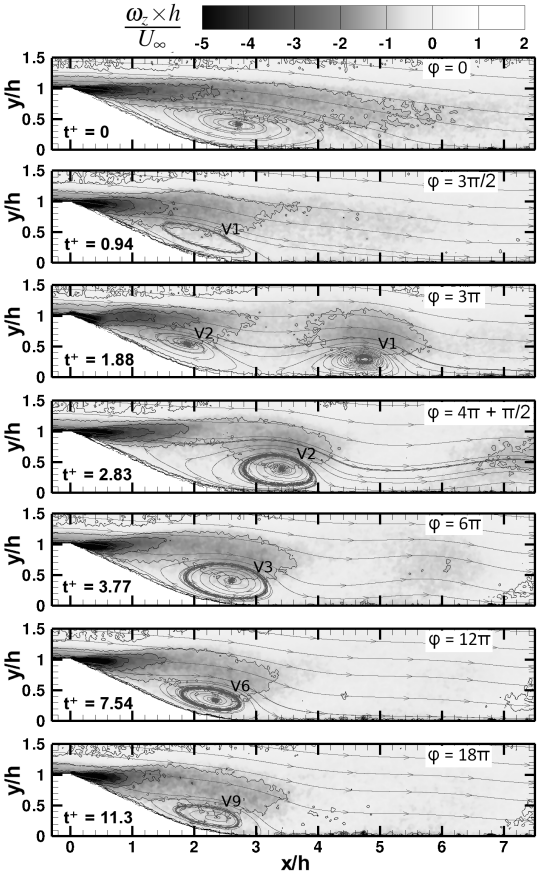

Figure 12. Phase averaged vorticity of attachment process. The AVG actuation is turned on at $t^+ = 0$. Phase blowing is specified using φ. $\varphi \equiv (\text{mod } 2\pi)$ corresponds to beginning of blowing phase while $\varphi \equiv \pi(\text{mod } 2\pi)$ is the end of blowing phase. Vi corresponds to the structure induced by the i^{th} AVG blowing phase.

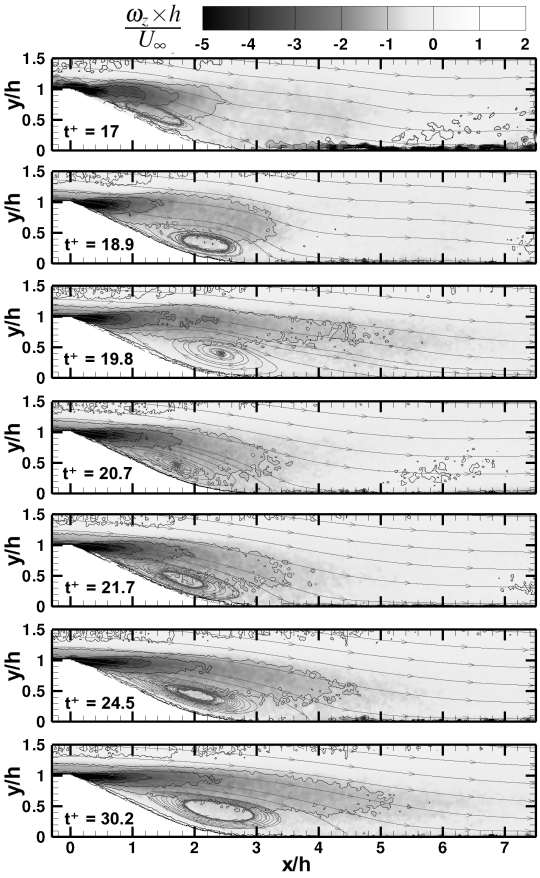

Figure 13. Phase-averaged vorticiy of separation process. The AVG actuation is turned off for $t^+ > 18$.

each AVG blowing phase is responsible for the generation of a spanwise structure. The first blowing AVG phase induces a large spanwise structure (see $t^+ = 0.94$, $x/h = 2.1; y/h = 0.44$) which increases the diffusion of the vorticity sheet. This induces the thickening of the vorticity sheet downstream of the sharp edge and a faster decrease of vorticity level in the streamwise direction. As observed at $t^+ = 1.88$ ($x/h = 4.74; y/h = 0.29$), this first spanwise vortex remind up to the initial location of mean attachment point ($x/h = 5.2$, $t^+ \leq 0$) and a residual vorticity convected by this first vortex remains above $x/h = 7.2$ at $t^+ = 2.83$. It appears that the circulation of following spanwise vortices induced by AVG blowing is lost farther upstream, with a faster decrease of their lumped vorticity. Furthermore, the second and third vortices induced by AVG blowing present a large size, with a height close to the height of the ramp. Those large scale vortices disappear for the next generations induced by AVG (see for instance $t^+ = 7.54$ or $t^+ = 11.3$). The longer time life of the first spanwise vortex could be explained by the fact that no large coherent structure precedes this first vortex while the interaction between two consecutive vortices is expected to lead a faster decrease of lumped vorticity draws by the following shedding vortices. As explained by (Darabi & Wygnanski (2004*a*)), the volum-flow-rate crossing between two consecutive vortices is pointing away from the wall. This is due to the larger outward flow induced by the amplified downstream vortex. It can be expected that the outward flow of the downstream vortex will attenuate the upstream vortex circulation.

The first three large vortices can be explained as vortices induced by AVGs that would to be subjected to an amplification of a global instability (Darabi & Wygnanski (2004*a*)). The reduction of the vortex size observed after the first three vortices is expected to be due to a modification of the absolute instability region inducing the modification of vortex shedding amplification region.

As explained above, the transient separation phase presents a time scale of about $t^+ \approx 20$. As actuators are turned off, a pressure plateau remains for $\Delta t^+ \approx 2$ after the last vortex print (see figure 11) before to reach the pressure value corresponding to the non-controlled flow. The phase-averaged vorticity fields (figure 13) show that after the shed of the last induced AVG blowing structure ($t^+ = 18.9$), the vorticity layer is rapidly growing in the streamwise direction while a large separation zone appears, which deflects the shear layer towards the freestream flow ($t^+ = 19.8$, $1.3 \leq x/h \leq 2$). The next vorticity field ($t^+ = 20.7$) presents a transverse thickening and a streamwise reduction of the vorticity layer (*i.e.* $-0.2 \leq \frac{\omega_z \times h}{U_\infty} \leq -0.1$) while the higher level of vorticity is shifted farther downstream in the shear layer. This process seems similar to the dynamic stall vortex observed by Darabi & Wygnanski (2004*b*). From $t^+ = 20.7$ to $t^+ \approx 38$, the thickness of the vorticity layer progressively

decreases while the higher vorticity level progresses farther downstream up to achieve the non-controlled state.

CONCLUSION

The control of separation induced over a sharp edge ramp by AVG, designed with the help of Godard & Stanislas (2006) and Cuvier *et al.* (2011), has been investigated. Two AVG actuation frequencies were used that lead to roughly similar control performances. The results show that for both cases, drastic reduction of separation length was observed (41 and 48 %). Furthermore, the use of AVG actuation frequency close to the vortex shedding frequency exhibits a better decrease of separation length explained by a lock-on effect. This lock-on control inducing large spanwise vortices appears despite the original objective of AVG to produce streamwise vortices. Furthermore, the vorticity field shows that AVG blowing phases lead to a deflect of the vorticity layer along the ramp despite the sharp edge and the drastic slant angle which is expected due to the development of counter-rotating streamwise vortices. Nevertheless, a classical development of the shear layer occurs farther downstream and induces the spanwise roll-up process.

The transient processes of attachment and separation induced by turning on and off the actuators present dimensionless time scales $t^+ \approx 10$ and $t^+ \approx 20$, respectively. The attachment process is characterized by the generation of a large scale spanwise vortex, which was observed up to the non-controlled mean attachment point while the spanwise coherence of following vortices appear to be suppressed farther downstream. This was expected to be due to the volum-flow-rate crossing between two consecutive AVG originated vortices that pointing away from the wall. This induces a faster decrease of circulation and the destruction of the spanwise coherence, despite the convected signature of their residual prints observed in the wake using resolved pressure taps. Furthermore, the first three vortices generated by AVG present a large scale at the same order of magnitude as the ramp height, while the next vortices present smaller scale size. This size vortex reduction could be induced by the modification of the absolute instability zone as the separation area is shifted upstream.

After the last generation of AVG blowing structures, the separation process was characterized by a rapid increase of the recirculation zone, inducing the deflection of the shear layer, the shed of this first recirculation zone and the thickening of the shear layer. As high level of vorticity was located farther downstream in the shear layer, this later progressively deflected up to its non-controlled location.

Acknowledgements

This work was supported by French National Research Agency (ANR) in the context of SePaCoDe Project (ANR-11-BS09-018).

REFERENCES

Collis, S. Scott, Joslin, Ronald D., Seifert, Avi & Theofilis, Vassilis 2004 Issues in active flow control: theory, control, simulation, and experiment. *Progress in Aerospace Sciences* **40** (45), 237 – 289.

Cuvier, Christophe, Braud, Caroline, Foucaud, Jean-Marc & Stanislas, Michel 2011 Flow control over a ramp using active vortex generators. In *Seventh International Symposium on Turbulence and Shear Flow Phenomena*. Ottawa, Canada.

Darabi, A. & Wygnanski, I. 2004*a* Active management of naturally separated flow over a solid surface. part 1. the forced reattachment process. *Journal of Fluid Mechanics* **510**, 105–129.

Darabi, A. & Wygnanski, I. 2004*b* Active management of naturally separated flow over a solid surface. part 2. the separation process. *Journal of Fluid Mechanics* **510**, 131–144.

Debien, Antoine, Aubrun, Sandrine, Mazellier, Nicolas & Kourta, Azeddine 2014 Salient and smooth edge ramps inducing turbulent boundary layer separation: Flow characterization for control perspective. *Comptes Rendus Mecanique* **342** (67), 356 – 362, flow separation control.

Godard, G. & Stanislas, M. 2006 Control of a decelerating boundary layer. part 3: Optimization of round jets vortex generators. *Aerospace Science and Technology* **10** (6), 455 – 464.

Greenblatt, David & Wygnanski, Israel J. 2000 The control of flow separation by periodic excitation. *Progress in Aerospace Sciences* **36** (7), 487 – 545.

Gad-el Hak, Mohamed 2007 The taming of the shrew: Why is it so difficult to control turbulence? In *Active Flow Control* (ed. Rudibert King), *Notes on Numerical Fluid Mechanics and Multidisciplinary Design (NNFM)*, vol. 95, pp. 1–24. Springer Berlin Heidelberg.

Siauw, W.L., Bonnet, J.-P., Tensi, J., Cordier, L., Noack, B.R. & Cattafesta, L. 2010 Transient dynamics of the flow around a {NACA} 0015 airfoil using fluidic vortex generators. *International Journal of Heat and Fluid Flow* **31** (3), 450 – 459, sixth International Symposium on Turbulence and Shear Flow Phenomena.